A Nature Portfolio journal



https://doi.org/10.1038/s42005-025-02245-4

Cross-scale nonlinear interaction and bifurcation in multi-scale turbulence of high-temperature plasmas

Check for updates

Tokihiko Tokuzawa ^{1,2,3} ⊠, Tatsuhiro Nasu², Daiki Nishimura¹, Katsumi Ida¹, Mikirou Yoshinuma¹, Tatsuya Kobayashi¹,2,3, Kenji Tanaka¹,3, Shigeru Inagaki ¹, Akihide Fujisawa¹,3, Ichihiro Yamada¹ & Kimitaka Itoh⁵

The structural formation of magnetized high-temperature plasmas, which are ubiquitous in nature, is often controlled by turbulence. Such plasma turbulence is characterized by multiple scales and thus cross-scale nonlinear interactions are key to understanding its dynamics and structural formation. This is also the case for laboratory plasmas, for which multi-scale turbulence data are most abundant. The interactions of components on the meso- and ion-gyroradius (micro)-scales have been extensively studied. Here we report, the experimental discovery of the cross-scale nonlinear interactions between fluctuations at micro-scale and hyper-fine (HF)-scale (whose scale is about an electron gyroradius). Cross-scale bifurcation is found, in which micro-scale turbulence is suppressed, and the amplitude of HF-scale turbulence simultaneously increases. There is also an abrupt change in the isotropy of HF-scale components. We discuss a possible mechanisms in which nonlinear interactions, related to the weakening of the electric field generated by micro-scale turbulence, enhance HF-scale turbulence.

In the turbulence of magnetized high-temperature plasmas, fluctuation components at several scales coexist. Multi-scale turbulence studies have been actively conducted on laboratory¹ and space² plasmas. Studies on multi-scale turbulence in magnetically confined high-temperature plasmas³, for which detailed data are available, are particularly valuable because they provide fundamental knowledge essential for fusion reactor development.

Micro-scale (i.e., scale of ion gyroradius, ρ_i) instabilities in magnetically confined high-temperature plasmas and the turbulent transport driven by these instabilities have attracted much attention⁴. The coexistence of non-linearly excited meso-scale fluctuations (e.g., zonal flows)³ has also shed light on multi-scale turbulence. Hyper-fine (HF) scale turbulent fluctuations, such as those on scales near the collisionless skin depth^{5,6} and electron temperature gradient (ETG) mode⁷ turbulence, which is characterized by the electron gyroradius ρ_e , have been theoretically predicted. The existence of ETG instabilities has been confirmed in basic experimental plasmas at low temperatures^{8–10}. Although observations of HF-scale turbulence in magnetically confined high-temperature plasmas have been reported^{11–14}, there are few experimental studies compared to those on micro-scale turbulence.

Transport due to HF-scale turbulence has been considered insignificant based on the assumption that the diffusion coefficient $D \sim y/k_r^2$ (where

 γ is the growth rate and k_r is the radial wavenumber for the turbulence)⁴, with the order of magnitude of $k_r \rho_e$ estimated to be ~O(1). However, nonlinear simulations 15,16 and a theoretical analysis 17 pointed out the possibility that the ETG instabilities may have a short wavelength in the poloidal direction but a long and elongated structure (a kind of streamer) in the radial direction. That is, the quasi-linear model y/k_r^2 predicts the possibility of large transport. Another issue is that HF-scale turbulence may have completely different behavior from that of the previously-studied multi-scale turbulence¹⁸. That is, the authors of reference¹⁸ pointed out that HF-scale turbulence is stretched by micro-scale turbulence due to the nonlinear effects of cross-scale interactions. From this nonlinear coupling, two states can exist: one in which HF-scale turbulence is dominant and one in which micro-scale turbulence is dominant. A macroscopic non-uniform radial electric field can control which of the two states is realized, because it suppresses the low-wavenumber turbulence more effectively; as a result, it enhances the high-wavenumber turbulence by suppressing the lowwavenumber turbulence. These results are supported by a study on nonlinear effects that may induce streamers in ETGs¹⁹. In addition, nonlinear simulations that cover both the micro- and HF-scales have recently become available 20,21 . The results confirm the importance of coupling between

¹National Institute for Fusion Science, National Institutes of Natural Sciences, Toki, Japan. ²The Graduate University for Advanced Studies, SOKENDAI, Toki, Japan. ³Research Institute for Applied Mechanics, Kyushu University, Kasuga, Japan. ⁴Institute of Advanced Energy, Kyoto University, Gokasho, Uji, Japan. ⁵Chubu University, Kasugai, Japan. ⊠e-mail: tokuzawa@nifs.ac.jp

turbulence components at different scales. It is thus extremely important to experimentally observe the HF-scale turbulence component and to understand the mechanism of the cross-scale nonlinear interactions in which they are involved and their impact on turbulent transport. For example, in the transport barrier of H-mode plasma²², the strong inhomogeneity of the radial electric field suppresses ion-scale microinstabilities^{23–25}. The HF-scale turbulence component might play a key role in controlling the structure of the transport barrier in plasma density.

We previously observed HF-scale turbulence fluctuations in the high-temperature plasma of the Large Helical Device (LHD)²⁶ using a recently developed measurement method²⁷ and confirmed that these fluctuations substantially contribute to anomalous electron transport²⁸. In the present study based on our previous experimental progress, we report the results of experiments on cross-scale nonlinear interactions obtained by simultaneously measuring the cross-scale turbulence response at a given spatial location and also measuring the anisotropy of the HF-scale turbulence. A cross-scale bifurcation occurs in which the micro-scale turbulence is suppressed and simultaneously the amplitude of the HF-scale turbulence increases, and an abrupt change in the isotropy of the HF-scale component is also observed. Considering its fast time scale, this bifurcation is considered to be caused by the cross-scale interaction of the plasma turbulence.

Results

Experimental set-up

The experiments were conducted in the LHD. In the LHD, the magnetic field required for plasma confinement is entirely covered by the current supplied to the coils from the outside (i.e., no magnetic field from the current flowing through the plasma is required). The characteristics of plasma instability can thus be measured stably and reproducibly. Discharges with slowly increasing plasma density were used to investigate the onset of bifurcation phenomena and the response of turbulence under the following conditions: the magnetic axis position in the vacuum field was (R_{ax}) was 3.55 m, the magnetic field strength (B_t) was 1.0 T, the helical coil pitch parameter (γ_c) was 1.2538, and the ratio of the quadrature field (B_0) was 100%. For plasma heating, 0.35-MW electron cyclotron heating (ECH) and 15-MW neutral beam injection (NBI) were used. To study the cross-scale interactions of micro-scale turbulence and HF-scale turbulence, simultaneous measurements at a given spatial location are required. Such measurements can be conducted by operating a millimeter-wave backscattering (BS) system²⁷ in combination with a microwave Doppler reflectometer (DR) system^{29,30}. For example, under the experimental conditions shown in Fig. 1a, the 57-GHz frequency channel of the DR system was used to observe micro-scale turbulence ($k_{\perp} \rho_s \sim 1.5$) near R = 4.4 m from the plasma cutoff layer, and the BS system was used to observe HF-scale turbulence ($k_{\perp}\rho_s$ ~ 7.0) at the same location. Furthermore, the anisotropy of turbulence in the HF-scale component was investigated via the simultaneous observation of various wavenumber components using the receiving antennas of the BS system at the positions and in the directions indicated by k_s in Fig. 1c, d. The wavenumber vector for the turbulence observed at Receiver 1 is k_1 and that observed at Receiver 2 is k_2 ; these vectors have approximately the same magnitude and different directions. Anisotropy here refers to the anisotropy within the cross-section perpendicular to the magnetic field lines (i.e., the anisotropy with respect to the radial and poloidal directions).

Observation of bifurcation in turbulence state

Figure 2a–g respectively show the time evolutions of the heating power of ECH and NBI, plasma current, plasma stored energy, line-averaged electron density, electron temperature, and line emission of H_{α} . The plasma gradually increased in density after being started by ECH. The fluctuation of the H_{α} signal increased at around t=3.82~s. At this time, the micro-scale turbulence intensity decreased rapidly and the HF-scale turbulence intensity increased rapidly, as shown in Fig. 2j, k, respectively. Here, we refer to the state before this phenomenon occurs as state A and the state after it occurs as state B. The temperature and density profiles just before and after the bifurcation into these two states show no significant change, especially in the

edge region ($r_{\rm eff}/a_{99} > 0.8$, where, $r_{\rm eff}$ is the effective minor radius and a_{99} is the average minor radius in which 99% of the electron kinetic energy is confined), as shown in Fig. 3. The relative variation between the two turbulence components is shown in Fig. 4. The micro-scale turbulence decreases and the HF-scale turbulence increases at the instant of bifurcation (<5 ms). This phenomenon is described in this paper as a bifurcation in turbulence states between those with lower and higher amplitudes of HF-scale turbulence.

It should be noted that this bifurcation of turbulence states is associated with a change in the global properties of plasmas. As shown in Fig. 2g, the H_{α} signal, which indicates the loss of energy from the main plasma, shows a transition to grassy-edge-localized-mode (ELM)-like behavior $^{31-33}$ at the onset of the bifurcation of the turbulence states. To categorize the time scales involved, the bifurcation phenomenon occurs in a few milliseconds or less, whereas macroscopic parameters such as the core density and temperature change more slowly (a few ten to a hundred milliseconds) and the burst-like response of the H_{α} signal is faster than the energy confinement time but longer than the bifurcation time scale. The intermittent fluctuation of H_{α} signal may be evidence of enhanced radial transport caused by HF-scale turbulence at the plasma periphery after the bifurcation.

Although the causal relationship is not clear in this figure, one might conjecture that the decrease in micro-scale turbulence may have caused the increase in HF-scale turbulence. In other words, the cross-scale interactions induced the changes in the intensity of micro-scale turbulence and that of HF-scale turbulence, which was deformed and suppressed by the micro-scale turbulent eddies. This hypothesis is supported by the observation of turbulence anisotropy, as described below.

Anisotropy in HF-scale turbulences

Theories have predicted that HF-scale turbulence might produce directional structures, such as long radially elongated formations (e.g., streamers) or eddies stretched by velocity shear. In this study, the issue of whether the structure of turbulence changes before and after the bifurcation in the turbulence state was investigated by simultaneously observing turbulent wavenumber components in two directions (k_1 and k_2), as shown in Fig. 1c, d. In other words, the anisotropy was investigated by simultaneously observing the turbulence intensity of wavenumber k components with the same magnitude but different directions. As shown in Fig. 5a, b, the intensity of the HF-scale turbulence increased as the micro-scale turbulence decreased at around t = 4.27 s for both directional components, as was the case in the previous section. Furthermore, the ratio of the intensities due to the observed differences in wavenumber direction changed, with the HF-scale turbulence being more isotropic after the bifurcation as shown in Fig. 5c. That is, the intensity ratio (k_2/k_1) exceeds unity when the turbulent eddies are radially elongated and becomes unity when the turbulent eddies are isotopic.

When the micro-scale turbulence is strong before the bifurcation, the HF-scale turbulence is more anisotropic, and when the micro-scale turbulence is weak after the bifurcation, the HF-scale turbulence is more isotropic. This result qualitatively supports the theoretical model's depiction of HF-scale turbulence being stretched by the background turbulent eddies (i.e., the dynamic shearing by micro-scale turbulence model)¹⁸.

Discussion

We now discuss the possibility that dynamic shearing by micro-scale turbulence as described above could actually occur. In addition, we make comparisons with the shear effect of background flow.

First, we evaluate the rate of dynamic shearing by micro-scale turbulence. From the mixing length estimation based on the gyro-Bohm diffusion model⁴, the amplitude of micro-scale turbulence can be expressed as

$$rac{e\phi_m}{T}\simrac{
ho_i}{L}$$

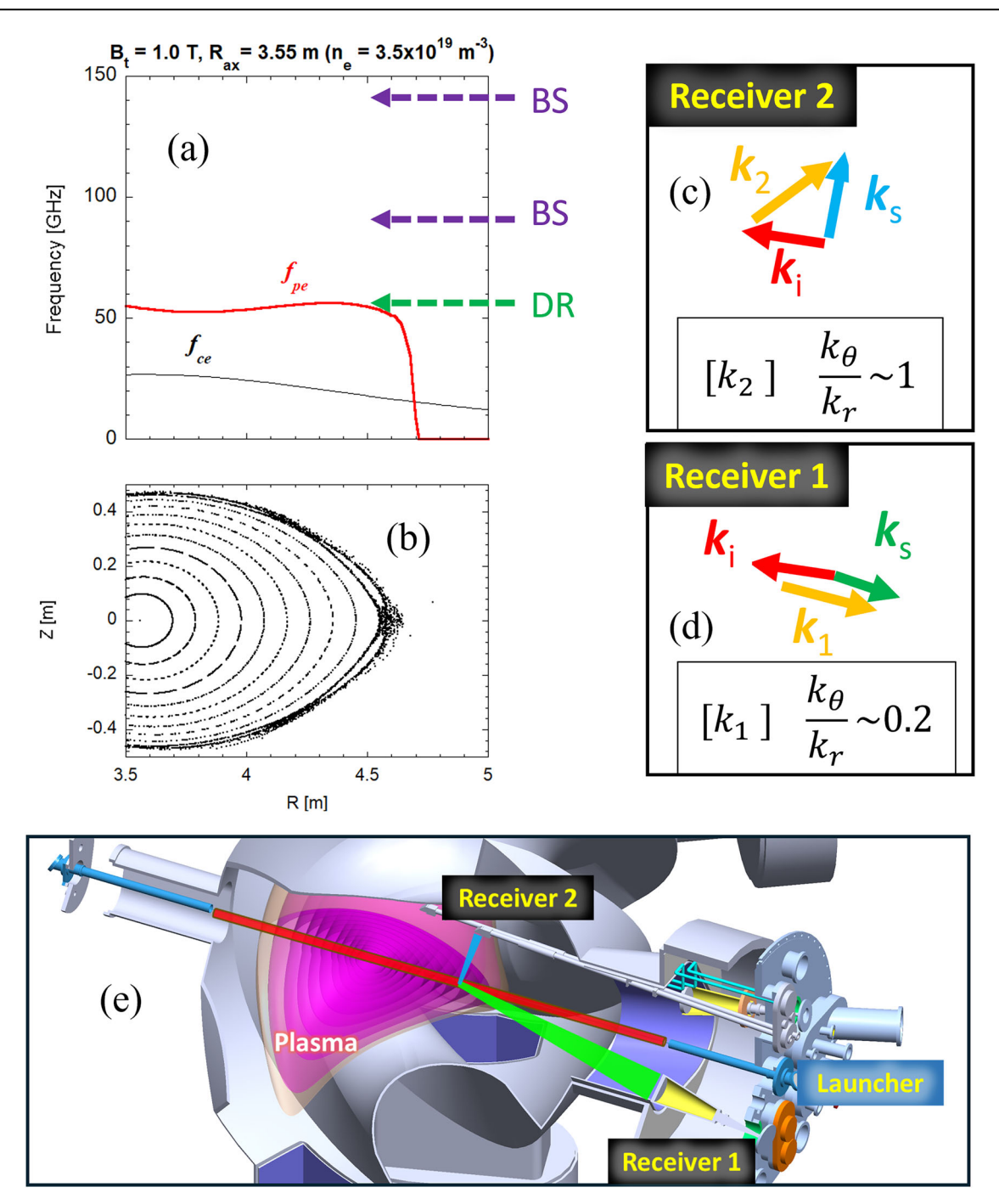


Fig. 1 | Coordination of multi-scale turbulence observations. a Radial profiles of electron cyclotron frequency $f_{\rm ce}$ and electron plasma frequency $f_{\rm pe}$. Probing wave frequencies of Doppler reflectometer (DR) and backscattering system (BS) are 57, 90, and 140 GHz, respectively. All waves use the ordinary polarized mode. **b** Magnetic flux surfaces in horizontal plasma cross-section with eye guide for each scattered wave ray. Relation between incident wave k_i and scattered wave k_s vectors at each BS receiving condition for (c) Receiver 2 and d Receiver 1. Here, k_r is the wavenumber in the radial direction and k_0 is the wavenumber in the poloidal direction. (e) Schematic diagram of backscattering antenna configuration. Probing

millimeter waves with frequencies of 90 and 140 GHz are injected from launcher antenna. The scattered waves are received by two antennas namely Receiver 1 and Receiver 2. Receiver 1 receives 90-GHz backscattered waves at about 160 degrees, consists of two metal lenses. It is movable, allowing the observation position to be changed. Receiver 2 is located above this cross-section and receives the scattered signal at about 70 degrees. It has a parabolic antenna at the tip and focuses the beam to $R=4.4\,\mathrm{m}$. In this experiment, Receiver 2 received millimeter waves at 140 GHz, making the wavenumbers received by the two antennas nearly the same. Here, the plasma shape is shown by the magnetic surface layers (pink region).

and the decorrelation rate γ_m of micro-scale turbulence can be assumed to take the following value:

$$\gamma_m \sim C_m V_{drift}/\rho_i$$

Here, e, ϕ_m , T, L, C_m , and V_{drift} are the electric charge, electrostatic potential, temperature, scale length of the global gradient, coefficients smaller than 1, and $E \times B$ drift velocity, respectively. The electric field E_m produced by the micro-scale turbulence eddies is estimated to be $E_m \sim \phi_m/\rho_i$. The shearing rate of HF-scale turbulence, V_m induced by this micro-scale

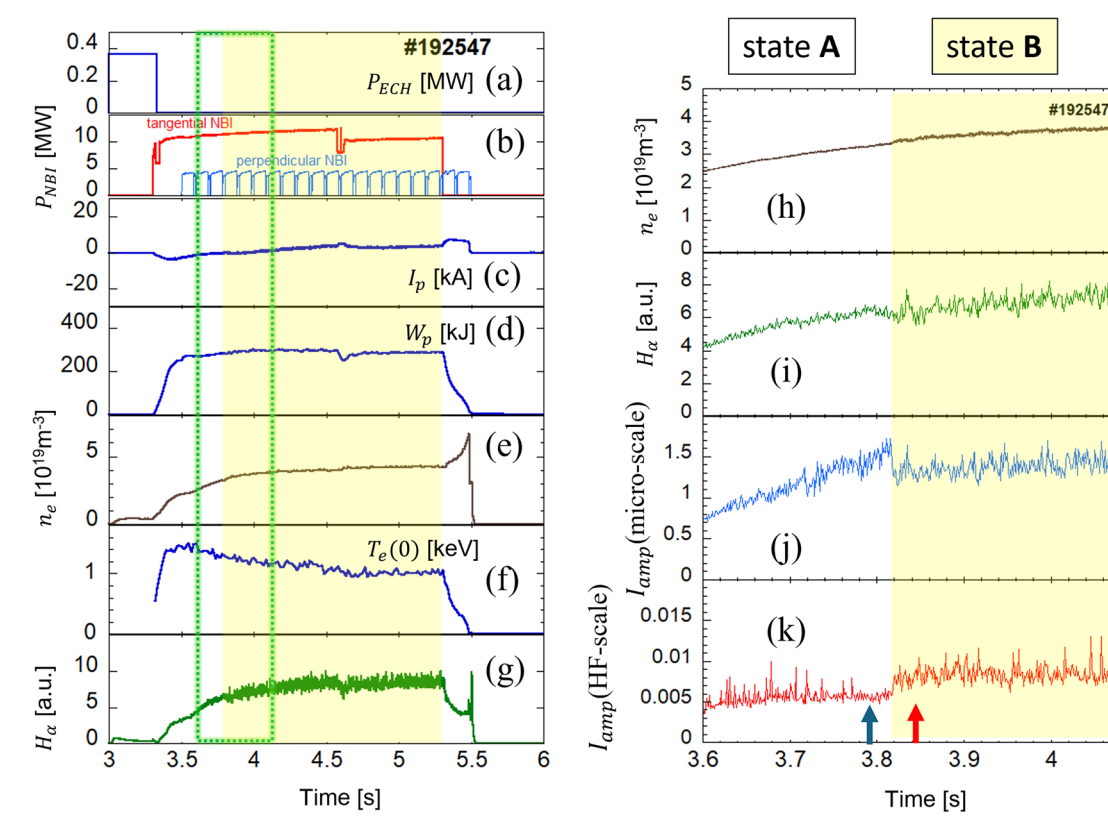


Fig. 2 | Temporal evolution of plasma parameters. The evolution of (a) ECH input power $P_{\rm ECH}$ and b tangential (red) and perpendicular (blue) NBI input power $P_{\rm NBI}$, c plasma current $I_{\rm p}$, d stored energy $W_{\rm p}$, e, h line-averaged electron density $n_{\rm e}$, f center electron temperature $T_{\rm e}$, g, i light emission of $H\alpha$ line, j micro-scale turbulence intensity $I_{\rm amp}$ (micro-scale), and k HF-scale turbulence intensity $I_{\rm amp}$ (HF-

scale). Graphs on right show magnified views of regions enclosed by green dotted line in graphs on left. State A is before the bifurcation, which occurred at around 3.82 s, and state B is after the bifurcation. The radial profiles at pre- and post-bifurcation times, indicated by blue and red arrows, are shown in Fig. 3.

4.1

turbulence, is evaluated as follows:

$$V_m' \sim rac{V_{drift}}{
ho_i}$$

Based on the plasma condition ($T_i = T_e = 200 \text{ eV}$, B = 0.65 T) at the time of turbulence bifurcation in this experiment, we obtain, $L = 7.6 \times 10^{-2}$ m, and $\rho_i = 2.2 \times 10^{-3}$ m.

Next, we investigate the decorrelation rate of the HF-scale turbulence obtained in the experiment, which is compared to the shearing rate caused by the micro component. Fig. 6 shows the auto correlation function of HF-scale turbulence during state A. The decorrelation rate can be estimated as the inverse of the decorrelation time, which is about $4\times10^4\,\mathrm{s}^{-1}$. The estimated electric field produced by the micro-scale turbulence eddies E_m is about 0.1–1 kV/m and its shearing rate is on the order of 10^4 – $10^5\,\mathrm{s}^{-1}$. Thus, the estimated decorrelation rate is well within the range where this dynamic shearing caused by micro-scale turbulence can be effective.

This argument is compared to the suppression by a background DC electric field. When the radial electric field E_r changes and $E_r \times B$ flow shear $V_{E\times B}$ becomes larger than γ_m , the micro-scale turbulence, which acts as a trigger for bifurcation is considered to be suppressed²³. However, the effect of this radial electric field on the HF-scale turbulence is relatively small because it needs to be (ρ_i/δ) times stronger than that for the micro-scale turbulence to suppress the HF-scale turbulence. Here, δ is the scale length of the HF-scale turbulence. Note that the E_r distribution could not be measured accurately in this experiment; this is a topic for future work.

The results show that, the suppression mechanism by the micro-scale component is highly plausible and important for the dynamics of the HF-scale component.

Conclusions

In this experimental study, we succeeded in simultaneously measured the micro-scale turbulence and the HF-scale turbulence, as well as the anisotropy of the HF-scale turbulence, at a given spatial location. The main results can be summarized as follows.

(i) A bifurcation in the turbulence state occurs between the micro-scale turbulence and the HP-scale turbulence. When this bifurcation occurs, the amplitude of the micro-scale component decreases rapidly and that of the HF-scale component increases rapidly. Before the bifurcation, the anisotropy of the HF-scale component is large (deformed by the micro-scale component). After the bifurcation, however, the anisotropy becomes smaller. This turbulence bifurcation qualitatively supports the theoretical depiction ¹⁸. Associated with this turbulence bifurcation, the plasma shows the change to grassy-ELM-like feature.

(ii) The decorrelation rate of the HF-scale component was estimated. The degree of deformation due to a vortex motion of the micro-scale component, as evaluated by the commonly used mixing length model, was found to be as large as or larger than the experimentally measured decorrelation rate of the HF-scale component. The suppression mechanism by the micro-scale component is highly plausible and important for the dynamics of the HF-scale component.

(iii) The experimental results show that it is essential to study cross-scale nonlinear interactions, including those of micro- and HF-scale components.

In addition, we found anotherphenomenon involving seesaw oscillation of the turbulence intensity at both scales in experiments with lower density and stronger electron heating than in this study, which will be reported in a future paper. In the near future, we plan to increase the number of spatial observation points and the number of observed wavenumber components to obtain wavenumber spectra and measure the radial electric

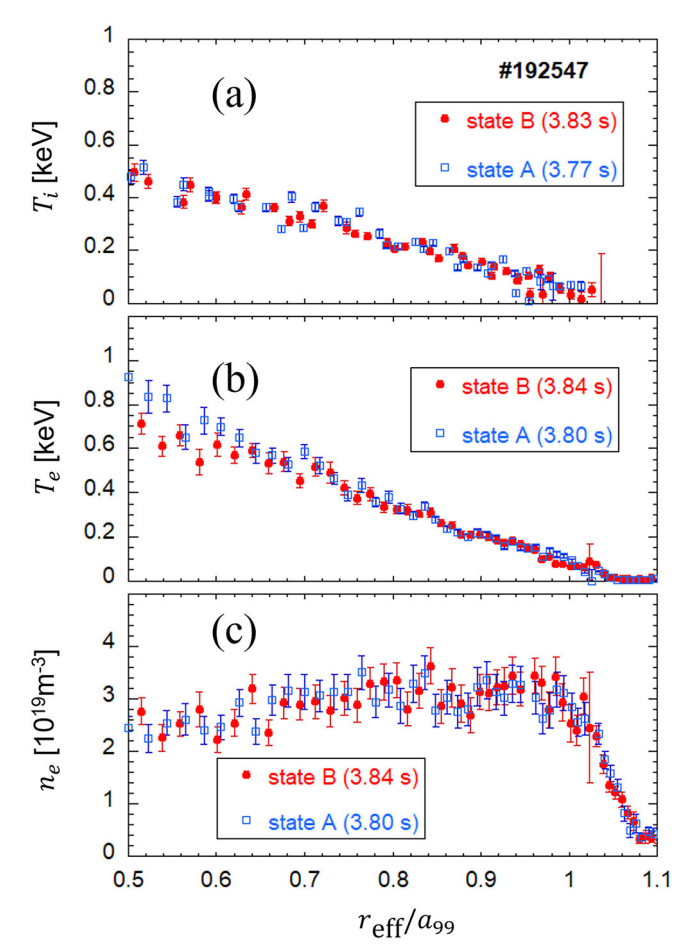


Fig. 3 | Radial profiles of temperature and density before and after bifurcation. Radial profiles of (a) ion temperature $T_{\rm i}$, b electron temperature $T_{\rm e}$, and c electron density $n_{\rm e}$ before (state A) and after (state B) bifurcation. Error bars show the standard deviation of each parameter.

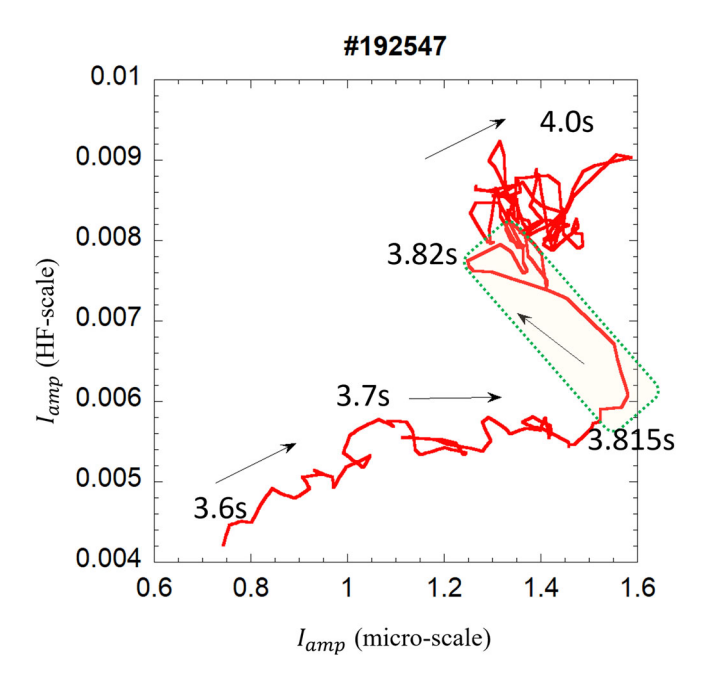


Fig. 4 | **Response relationship of turbulence intensities before and after the bifurcation.** Relationship between micro-scale turbulence intensity and HF-scale turbulence intensity. The numbers in the figure show time. The time period in which the bifurcation occurred (from 3.815 to 3.820 s) is indicated by the green dotted line.

field with high precision to develop a more detailed understanding of physical phenomena.

Methods

Large helical device

The Large Helical Device is a heliotron type device for the magnetic confinement of high-temperature plasmas. The representative major and minor radii of the torus plasma are 3.75 and ~0.6 m, respectively. The confinement magnetic field is mainly produced by the external helical coils; therefore, the plasma current need not be maintained. The plasma shape can be controlled by the quadrupole magnetic coils. The percentage cancellation of the quadrupole component, B_{cr} , is less than 100% when the plasma cross-section becomes elongated vertically. The plasma shape can also be controlled by the helical pitch parameter defined as $\gamma_c = (m/l)(a_c/R_c)$, where m, l, a_c , and R_c are the toroidal pitch number, poloidal pitch number, and average minor and major radii of the helical coils, respectively. For an LHD-type (l=2, m = 10) heliotron system, γ_c corresponds to the inverse aspect ratio of the helical coils (a_c/R_c) and $\gamma_c = 1.2538$ is the standard configuration. The magnetic field strength is up to 2.8 T. The device can be used to perform experiments in a variety of magnetic field configurations. The LHD features a total of five gyrotrons with frequencies of 56, 77, and 154 GHz for electron cyclotron heating. In this experiment, only the 56-GHz gyrotron was used for the plasma startup. The plasma was also heated by five neutral beams: three were tangentially injected and two were perpendicularly injected. Vertical neutral beam injection was also used to diagnose the ion temperature $T_{\rm i}$, perpendicular velocity $V_{\rm p}$, and radial electric field $E_{\rm r}$ measurements. The total port-through power was ~20 MW. In this experiment, the plasma density was $1-4 \times 10^{19} \,\mathrm{m}^{-3}$ and the central temperature was about 1 keV.

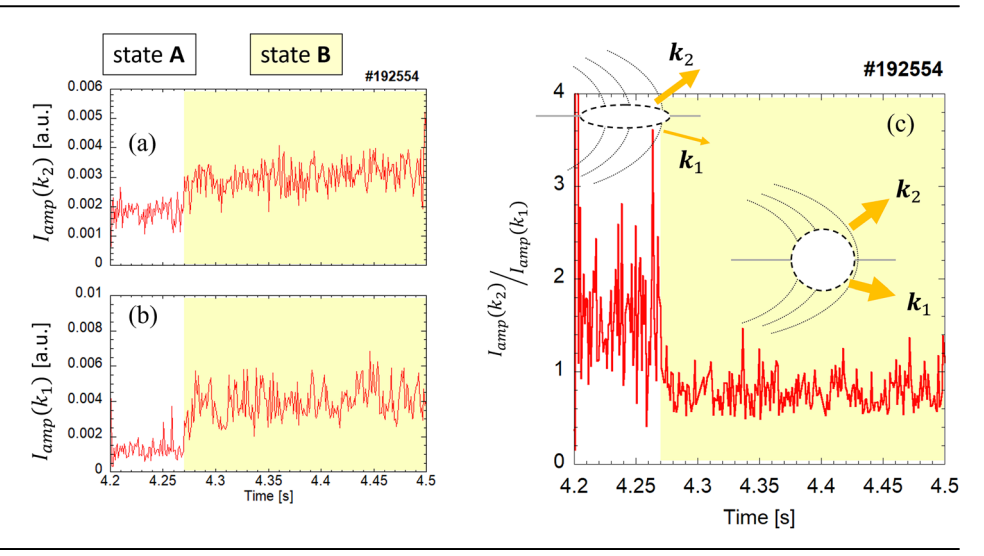
Millimeter-wave back-scattering measurement

A 90-GHz (W-band) and 140-GHz (D-band) millimeter-wave backscattering system was used to measure HF-scale turbulence characterized by collisionless skin depth and the electron gyroradius ρ_e . This system is crucial for accurately detecting the intensity of the scattered signal, which correlates with the square of the fluctuations in electron density within the plasma^{34,35}. The system consists of one transmitting antenna and two receiving antennas placed inside the LHD vacuum vessel, as shown in Fig. 1(e). To achieve high spatial resolution in these measurements, one of the receiving antennas had collinear focusing optics with metal lenses and the other had focusing optics with a rotating parabolic mirror. This setup kept the beam diameter below 30 and 50 mm, respectively. The collinear antenna (Receiver 1) design facilitates the adjustment of the observation position from the plasma core to its edge by means of a remote steering mechanism. The scattering volume's estimated size is approximately 100 mm at the plasma edge. This dimension corresponds to a length of approximately 0.1 in terms of r_{eff}/a_{99} . The receiving antenna with a parabolic mirror (Receiver 2) is fixed to the vacuum vessel to observe at $R = 4.4 \,\mathrm{m}$. In addition, the millimeter-wave heterodyne detection circuit within this system incorporates a modulation function. This function is pivotal for distinguishing and identifying noise components in the scattered signal. These noise components are primarily attributed to the cyclotron radiation emitted by electrons from the plasma, making this function essential for precise signal analysis.

Microwave Doppler reflectometer

Doppler reflectometry (DR)^{35–37} can measure density fluctuations with sensitivity to ion-gyroradius ρ_i scale turbulence. The perpendicular flow velocity, radial electric field, and perpendicular wavenumber spectrum within the range $k_{\perp}=2-20~{\rm cm}^{-1}$ as determined by the Bragg condition can be simultaneously observed with high wavenumber and spatial resolution. Since the observation position is determined by the position of the cutoff layer corresponding to the microwaves emitted into the plasma, to measure turbulence at various positions, the LHD applies a multi-frequency channel DR system that uses the frequency comb method. This system has sufficient time resolution and allows simultaneous multi-point spatial measurements.

Fig. 5 | Anisotropy of turbulence. Temporal behavior of HF-scale turbulence intensities in observed signals of (a) Receiver 2 and b Receiver 1. Here, the wavenumber k_2 and k_1 observed by Receiver 2 and Receiver 1 are wavenumber components in the directions shown in Fig. 1c, d, respectively. c Time variation of ratio of signal intensities in panels (a) and (b). The dotted ellipses are eye guides indicating the deformation of the HF-scale turbulent eddies, and the inclination of the propagation direction with respect to the magnetic surface before and after the bifurcation. After the bifurcation, the isotropy is recovered.



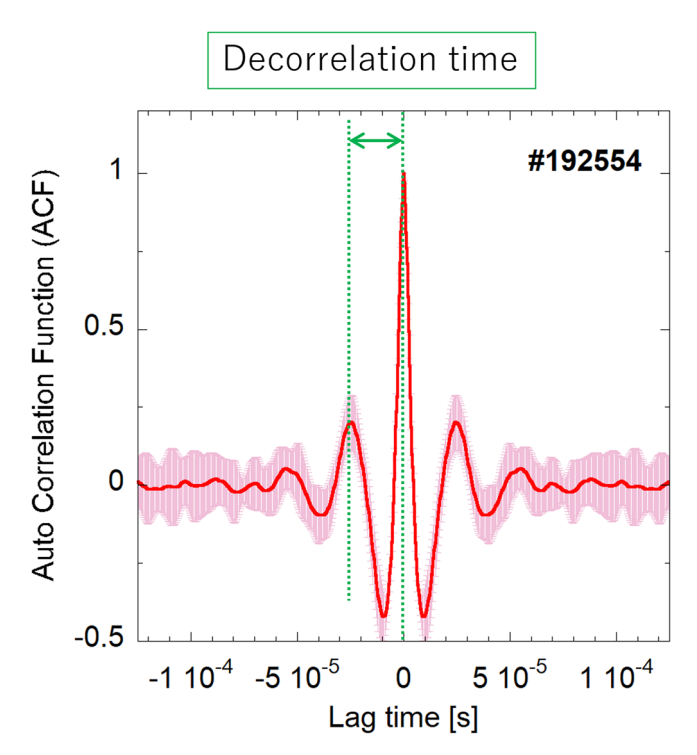


Fig. 6 | **Estimation of decorrelation rate.** Auto correlation function of HF-scale turbulence in state A. The mean value calculated every 1 ms during 20 ms is shown by the red line and the standard deviation is shown by the error bar. The decorrelation time was defined as the time to the first peak $(2.5 \times 10^{-5} \, \text{s})$ and its reciprocal was estimated as the decorrelation rate.

At the same toroidal position as that of the BS, both Ka-band and U-band DR systems are operated, allowing observation of the same plasma cross-section.

Data availability

Received: 14 January 2025; Accepted: 28 July 2025; Published online: 06 October 2025

References

- Fujisawa, A. et al. Experimental progress on zonal flow physics in toroidal plasmas. *Nucl. Fusion* 47, S718–S726 (2007).
- Hasegawa, H. et al. Transport of solar wind into Earth's magnetosphere through rolled-up Kelvin–Helmholtz vortices. *Nature* 430, 755 https://www.nature.com/articles/nature02799 (2004).
- Diamond, P. H., Itoh, K., Itoh, S.-I. & Hahm, T. S. Zonal flows in plasma-a review. Plasma Phys. Control. Fusion 47, R35 (2005).
- 4. Kadomtsev, B. B. Plasma Turbulence. (Academic, New York, 1965).
- Ohkawa, T. A transport model for alcator scaling in tokamaks. *Phys. Lett. A* 67, 35–38 (1978).
- Parail, V. V. & Pogutse, O. P. JETP Letters 32, 384. Proc. Blh Inl. Conf: on Piasma Physics and Controlled Nuclear Fusion Rerearch (Brmseh, 1980) 1 (Vienna: IAEA) p67 (1980).
- Horton, C. W. Drift waves and transport. Rev. Mod. Phys. 71, 735 (1999).
- Sokolov, V. & Sen, A. K. Measurements of electron thermal transport due to electron temperature gradient modes in a basic experiment. *Phys. Rev. Lett.* **107**, 155001 (2011).
- Mattoo, S. K. et al. Experimental observation of electron-temperaturegradient turbulence in a laboratory plasma. *Phys. Rev. Lett.* 108, 25507 (2012).
- Moon, C., Toshiro, K. & Hatakeyama, R. Dynamics of nonlinear coupling between electron-temperature-gradient mode and driftwave mode in linear magnetized plasmas. *Phys. Rev. Lett.* 111, 115001 (2013).
- Mazzucato, E. et al. Short-scale turbulent fluctuations driven by the electron-temperature gradient in the national spherical torus experiment. *Phys. Rev. Lett.* **101**, 075001 (2008).
- Ruiz, J. R. et al. Validation of gyrokinetic simulations in NSTX and projections for high-k turbulence measurements in NSTX-U. *Phys. Plasmas* 27, 122505 (2020).
- Rhodes, T. L. et al. Response of multiscale turbulence to electron cyclotron heating in the DIII-D tokamaka. *Phys. Plasmas* 14, 056117 (2007).
- Ren, Y. et al. Transport from electron-scale turbulence in toroidal magnetic confinement devices. Rev. Mod. Plasma Phys. 8, 5 (2024).
- Dorland, W., Jenko, F., Kotschenreuther, M. & Rogers, B. N. Electron temperature gradient turbulence. *Phys. Rev. Lett.* 85, 5579 (2000).
- Idomura, Y., Wakatani, M. & Tokuda, S. Stability of ExB zonal flow in electron temperature gradient driven turbulence. *Phys. Plasmas* 7, 3551 (2000).
- Gao, Z. et al. Temperature gradient driven short wavelength modes in sheared slab plasmas. *Phys. Plasmas* 10, 2831–2839 (2003).

- Itoh, S.-I. & Itoh, K. Statistical theory and transition in multiple-scalelength turbulence in plasmas. *Plasma Phys. Contr. Fusion* 43, 1055–1102 (2001).
- Holland, C. & Diamond, P. H. On the dynamics of large-scale structures in electron temperature gradient turbulence. *Phys. Lett. A* 344, 369–382 (2005).
- Maeyama, S. et al. Multi-scale turbulence simulation suggesting improvement of electron heated plasma confinement. *Nat. Commun.* 13, 3166 (2022).
- Maeyama, S. et al. Overview of multiscale turbulence studies covering ion-to-electron scales in magnetically confined fusion plasma. *Nucl. Fusion* 64, 112007 (2024).
- Wagner, F. et al. Regime of improved confinement and high beta in neutral-beam-heated divertor discharges of the ASDEX Tokamak. Phys. Rev. Lett. 49, 1408 (1982).
- 23. Biglari, H., Diamond, P. H. & Terry, P. W. Influence of sheared poloidal rotation on edge turbulence. *Phys. Fluids* **B 2**, 1–4 (1990).
- Shesterikov, I. et al. Experimental evidence for the intimate interaction among sheared flows, eddy structures, reynolds stress, and zonal flows across a transition to improved confinement. *Phys. Rev. Lett.* 111, 055006 (2013).
- Carter, T. A. & Maggs, J. E. Modifications of turbulence and turbulent transport associated with a bias-induced confinement transition in the Large Plasma Device. *Phys. Plasmas* 16, 012304 (2009).
- Takeiri, Y. et al. Extension of the operational regime of the LHD towards a deuterium experiment. *Nucl. Fusion* 57, 102023 (2017).
- Tokuzawa, T. et al. W-band millimeter-wave back-scattering system for high wavenumber turbulence measurements in LHD. Rev. Sci. Instrum. 92, 043536 (2021).
- Nasu, T. et al. Electron-scale turbulence characteristics with varying electron temperature gradient in LHD. Nucl. Fusion 64, 096008 (2024).
- Soga, R. et al. Developments of frequency comb microwave reflectometer for the interchange mode observations in LHD plasma. *J. Instrum.* 11, C02009 (2016).
- Tokuzawa, T. et al. Ka-band microwave frequency comb doppler reflectometer system for the large helical device. Plasma Fusion Res. 9, 1402149 (2014).
- Zohm, H. Edge localized modes (ELMs). Plasma Phys. Control. Fusion 38, 105 (1996).
- Suttrop, W. The physics of large and small edge localized modes. Plasma Phys. Control. Fusion 42, A1 (2000).
- Aiba, N. & Oyama, N. Numerical analysis of key factors for the appearance of grassy ELMs in tokamak plasmas. *Nucl. Fusion* 52, 114002 (2012).
- Froula, D. H. et al. Plasma scattering of electromagnetic radiation. Academic Press (2011). https://doi.org/10.1016/C2009-0-20048-1 (2011)
- Hartfuss, H.-J., & Geist, T. Fusion plasma diagnostics with mmwaves. Wiley (2013). https://doi.org/10.1002/9783527676279 (2013)
- Hirsch, M. et al. Doppler reflectometry for the investigation of propagating density perturbations. *Plasma Phys. Control. Fusion* 43, 1641–1660 (2001).
- Conway, G. D. et al. Direct measurement of zonal flows and geodesic acoustic mode oscillations in ASDEX Upgrade using Doppler reflectometry. *Plasma Phys. Control. Fusion* 47, 1165–1185 (2005).

Acknowledgements

We thank the LHD experiment group for their support of this work. This paper is dedicated to the memory of the late Professor Sanae-I. Itoh. In particular, we salute her for opening up important new avenues for the study and understanding of plasma turbulence. This study was supported in part by the Japan Society for the Promotion of Science KAKENHI (grant nos. 19H01880, 21H04973, 23H01161, 23K25858, and 24K06997), by a budgetary Grant-in-Aid from the National Institute for Fusion Science (NIFS) LHD project under the auspices of the NIFS Collaboration Research Program, and by the Collaborative Research Programs of the Research Institute for Applied Mechanics, Kyushu University. Additional support was provided by Japan/U.S. Cooperation in Fusion Research and Development.

Author contributions

T.T., K.I., S.I., and A.F. conceived the experiment. T.T., T.N., and D.N. conducted the experiment. K.I., M.Y., T.K., K.T., I.Y., and K. Itoh analyzed the data. T.T. and K. Itoh drafted the article. All authors contributed to discussions and the interpretation of the results, and confirmed the manuscript.

Competing interests

The authors declare no competing interests.

Additional information

Correspondence and requests for materials should be addressed to Tokihiko Tokuzawa.

Peer review information Communications Physics thanks Xijie Qin, Lothar Schmitz and the other, anonymous, reviewer(s) for their contribution to the peer review of this work.

Reprints and permissions information is available at

http://www.nature.com/reprints

Publisher's note Springer Nature remains neutral with regard to jurisdictional claims in published maps and institutional affiliations.

Open Access This article is licensed under a Creative Commons Attribution-NonCommercial-NoDerivatives 4.0 International License, which permits any non-commercial use, sharing, distribution and reproduction in any medium or format, as long as you give appropriate credit to the original author(s) and the source, provide a link to the Creative Commons licence, and indicate if you modified the licensed material. You do not have permission under this licence to share adapted material derived from this article or parts of it. The images or other third party material in this article are included in the article's Creative Commons licence, unless indicated otherwise in a credit line to the material. If material is not included in the article's Creative Commons licence and your intended use is not permitted by statutory regulation or exceeds the permitted use, you will need to obtain permission directly from the copyright holder. To view a copy of this licence, visit https://creativecommons.org/licenses/by-nc-nd/4.0/.

© The Author(s) 2025